Exp Fluids
DOI 10.1007/s00348-006-0238-2

RESEARCH ARTICLE

On the Lamb vector and the hydrodynamic charge

Germain Rousseaux · Shahar Seifer · Victor Steinberg · Alexander Wiebel

Received: 8 June 2006 / Revised: 3 October 2006 / Accepted: 18 November 2006

Abstract This work is an attempt to test the concept of the hydrodynamic charge (analogous to the electric charge in electromagnetism) in the simple case of a coherent structure such as the Burgers vortex. We provide experimental measurements of both the so-called Lamb vector and its divergence (the charge) by two-dimensional particles images velocimetry. In addition, we perform a Helmholtz–Hodge decomposition of the Lamb vector in order to explore its topological features. We compare the charge with the well-known Q-criterion in order to assess its interest in detecting and characterizing coherent structure. Usefulness of this concept in studies of vortex dynamics is demonstrated.

1 Introduction

One of the crucial issues in turbulence is related to the identification of the so-called coherent structures in complex flows. These structures are characterized by a spatial concentration of vorticity, a life time much longer than the period of rotation (or turn-over time) and by their unpredictability. Several criteria, which do not focus on the vorticity distribution per se, have been introduced in the literature for the purpose of detecting coherent structures. However, no consensus has been reached so far (Weiss 1991; Haller 2005). Recently, the notion of ''Q-criterion'' (or Weiss determinant) was introduced in order to characterize turbulent flows mainly in numerical simulations: one calculates the Laplacian of the dynamic pressure alone to visualize the coherent structures (Dubief and Delcayre 2000; Lesieur et al. 2003). Besides, a vortex is characterized by a low pressure in its centre and its core exhibits a local velocity minimum. Indeed, the experiments of Douady et al. (1991) on the visualization of coherent structures in a turbulent flow by injecting air bubbles in water show that the bubbles do accumulate in the centre of the structures that is in the pressure minima (see also the numerical simulations of Pumir (1994)), which correspond to the vorticity maxima. These authors have pointed out the analogy between the Q-criterion and the electric charge in classical electromagnetism.

The goal of our paper is to validate experimentally a criterion based on the so-called ''hydrodynamic charge'' with the help of an analogy between fluid mechanics and electromagnetism dating back to Maxwell, to compare it with the Q-criterion, and to demonstrate the interest of the new criterion to study vortex dynamics. In particular, we aim at demonstrating the usefulness of this concept associated to the mapping of the so-called ''Lamb vector'' in order to characterize the vortex core and structure. According to our knowledge, there are almost no experimental

G. Rousseaux (✉)
Institut Non-Linéaire de Nice, UMR 6618 CNRS-UNICE,
Université de Nice-Sophia Antipolis,
1361 route des Lucioles, 06560 Valbonne, France
e-mail: Germain.Rousseaux@inln.cnrs.fr

S. Seifer · V. Steinberg
Department of Physics of Complex Systems,
Weizmann Institute of Science,
76100 Rehovot, Israel

A. Wiebel
Institut für Informatik, Universität Leipzig,
PF 100920, 04009 Leipzig, Germany

measurements of the Lamb vector as well as the hydrodynamic charge.

2 The Lamb vector and the hydrodynamic charge

2.1 Theoretical background

The Navier–Stokes equation for incompressible flow ($\nabla.\mathbf{u} = 0$) can be written in a form that was given, among others, by Lamb (1878):

$$\partial_t \mathbf{u} = -\nabla\left(\frac{p}{\rho} + \frac{\mathbf{u}^2}{2}\right) - 2\boldsymbol{\Omega} \times \mathbf{u} - \nu\nabla \times \mathrm{w},$$

where $\Omega = \mathbf{w}/2$ is the vortex vector ($\mathbf{w} = \nabla \times \mathbf{u}$ is the vorticity) which is analogous to the angular velocity of solid rotation in solid mechanics. The Lamb vector $\mathbf{l} = \mathbf{w} \times \mathbf{u} = 2\Omega \times \mathbf{u}$ (we can find also the expression ''vortex force'' in the literature to denote this vector) represents the Coriolis acceleration of a velocity field under the effect of its own rotation (usually for solid body rotation, the Coriolis force is built with a rotation vector which is independent of the velocity).

Under the incompressibility constraint ($\nabla.\mathbf{u} = 0$), Marmanis and Shridar have proposed independently a set of ''hydrodynamic Maxwell equations'' which takes the form (Marmanis 1998, Kirby et al. 1999, Shridar 1998):

$$\nabla.\mathbf{w} = 0 \text{ or } \mathbf{w} = \nabla \times \mathbf{u}$$

$$\partial_t \mathbf{w} = -\nabla \times \mathbf{l} - \nu\nabla \times \nabla \times \mathbf{w} \text{ or } \mathbf{l}$$
$$= -\partial_t \mathbf{u} - \nabla\left(\frac{p}{\rho} + \frac{\mathbf{u}^2}{2}\right) - \nu\nabla \times \mathbf{w}$$

$$\nabla.\mathbf{l} \equiv q_H = -\nabla^2\left(\frac{p}{\rho} + \frac{\mathbf{u}^2}{2}\right)$$

where q_H is the so-called ''hydrodynamic charge density''.

The first equation stands for the conservation of the vorticity flux along a tube of vorticity. It implies the absence of monopole source of vorticity as a vorticity tube that wraps on itself, goes to infinity or is connected to the walls of the flow volume. One finds the second and third equations by taking respectively the curl and divergence operators of the Navier–Stokes equation. The second one illustrates that the temporal variation of the angular velocity is equal to the torque exerted by the Coriolis force that is the Lamb vector. The third one shows that the sources of the Lamb vector are the pressure and velocity gradients.

The hydrodynamic charge can be seen as a topological feature of the flow. Indeed, it is expressed mathematically by the ''curvature'' (second derivative) of the sum of potential (pressure) and kinetic energies. As a matter of fact, the Laplacian operator was defined by James Clerk Maxwell in his famous Treatise (Clerk Maxwell 1873) (volume 1, article 26) as the ''concentration'' of a quantity since it indicates the excess of the value of the quantity over its mean value in the neighborhood of the point. Vortices are topological concentration of energy (both potential and kinetic). One notices that the charge vanishes where the flow is irrotational ($\mathbf{w} = \mathbf{0}$ implies $\mathbf{l} = \mathbf{0}$). There exist localized topological structures associated with a charge that correspond to vorticity filaments, vortices, and, more generally, to the coherent structures.

One can resume the analogy due to Marmanis (1998) and Shridar (1998) with a table. Each electromagnetic property has an hydrodynamic counterpart:

Hydrodynamical quantities	Electromagnetic quantities
Specific enthalpy p/ρ	Scalar potential V
Velocity $\mathbf{u}$	Vector potential $\mathbf{A}$
Vorticity $\mathbf{w}$	Magnetic induction $\mathbf{B}$
Lamb vector $\mathbf{l}$	Electric field $\mathbf{E}$
Hydrodynamic charge q_H	Electric charge q_E

The Lamb vector can be seen as a ''motional'' electric field analogous to the so-called Lorentz electric field which appears during a Galilean transformation ($\mathbf{E}' = \mathbf{E} + \mathbf{v} \times \mathbf{B}$ and $\mathbf{B}' = \mathbf{B}$ are analogous to $\mathbf{l}' = \mathbf{l} + \mathbf{w} \times \mathbf{v}$ and $\mathbf{w}' = \mathbf{w}$). Moreover, the Lamb vector of a cylindrical vortex is radial like the electric field associated to a charged wire. That's why a vortex is a dual electromagnetic object as it is a tube of ''magnetic induction'', which carries an ''electric charge''.

One can separate the Lamb vector in two parts according to the so-called Helmholtz–Hodge decomposition (Wu et al. 1999a, b, 2005):

$$\mathbf{l} = \mathbf{l}_{//} + \mathbf{l}_{\perp} = \nabla\alpha + \nabla \times \beta \text{ with } \nabla.\beta = 0$$

The indexes // and $\perp$ correspond to the projections of the Lamb vector parallel (irrotational part) and perpendicular (solenoidal part) to the wave vector in the associated fourier space. One infers that the hydrodynamic charge is a function only of the parallel part $\mathbf{l}_{//}$ and the scalar α is completely determined by the incompressibility constraint ($\nabla.\mathbf{u} = 0$) :

$$\nabla.\mathbf{l} = \nabla.\mathbf{l}_{//} = -\nabla^2\left(\frac{p}{\rho} + \frac{\mathbf{u}^2}{2}\right) = \nabla^2\alpha = q_H$$

$$\text{where } \alpha = -\left(\frac{p}{\rho} + \frac{\mathbf{u}^2}{2}\right)$$

We notice now that the Navier–Stokes equation can be split in two parts:

$$\mathbf{l}_{//} = -\nabla\left(\frac{p}{\rho} + \frac{\mathbf{u}^2}{2}\right) \text{ and } \mathbf{l}_{\perp} = -\partial_t\mathbf{u} - \nu\nabla \times \nabla \times \mathbf{u}$$

The Helmholtz–Hodge decomposition of the Lamb vector is not, in general, unique as one can subtract simultaneously from $\mathbf{l}_{//}(\mathbf{E}_{//})$ and add to $\mathbf{l}_{\perp}(\mathbf{E}_{\perp})$ the gradient of a function, which is solution of a Laplace equation (see the numerical implementation below). For example, the vector potential (velocity) outside a solenoid (a Rankine vortex) derives from a harmonic function. Hence, its time derivative is a gradient that can enter into the longitudinal part. The boundary conditions are essential in order to guaranty uniqueness.

In the particular case of a stationary flow and when the viscous effects are negligible, the Navier–Stokes equations resume to the ''auto-strophic'' equilibrium (one speaks of geo-strophic equilibrium when the earth coriolis effect equilibrates the pressure gradient):

$$\mathbf{l} = \mathbf{w} \times \mathbf{u} = \mathbf{l}_{//} = \nabla\alpha$$

The Lamb vector is perpendicular to the surface of constant α and each of these surfaces features the streamlines and the vorticity lines (Sposito 1997): $\mathbf{w}.\nabla\alpha \equiv 0$ and $\mathbf{u}.\nabla\alpha \equiv 0$. This statement ceases to be true at Beltrami points where velocity and vorticity are parallel (Sposito 1997). In Electromagnetism, it would correspond to the motion along a magnetic field line: electrons are not influenced in this case.

Hence, the transverse component of the Lamb vector is equal to zero and this implies the existence of a relation between the stream function and the vorticity, which in 2D is equal to minus the Laplacian of the stream function (Lamb 1878). This property is very important in 2D turbulence, which features an inverse energy cascade from the small to the large scales of the flow. Indeed, in 3D turbulence, it is the transverse component of the Lamb vector, which is at the origin of the direct cascade of energy from the large to the small scales of the flow (Speziale 1989; Wu et al. 1999a,b). It can be shown that the longitudinal component is passive: its evolution is controlled by the transverse component (Wu et al. 1999a, b). In general, the transverse part is highly reduced in the region of space where the vorticity is concentrated (Shtilman 1992).

2.2 The Burgers vortex

The Burgers (Gaussian) vortex is a convenient model to derive the hydrodynamic charge of a typical single vortex. For comparison, in a Rankine vortex the Lamb field is discontinuous at the edge of the core and the charge diverges. We assume open cell, meaning that the characteristic radius of the Burgers vortex core, $r = a$, is much smaller than the cell radius. If Ω denotes the angular speed parameter of the vortex, the fields are expressed as follows (ν is the kinematic viscosity) (Wu et al. 2005):

$$\mathbf{u}.\mathbf{e}_r = -\frac{2\nu}{a^2}r$$

$$\mathbf{u}.\mathbf{e}_\theta = \mathbf{\Omega}\frac{a^2}{r}\left(1 - e^{-\frac{r^2}{a^2}}\right)$$

$$\mathbf{u}.\mathbf{e}_z = \frac{4\nu}{a^2}z$$

$$\mathbf{w} = 2\mathbf{\Omega}\mathrm{e}^{-r^2/a^2}\mathbf{e}_z$$

$$\mathbf{l} = \mathbf{l}_{//} + \mathbf{l}_{\perp} = w\mathbf{e}_z \times (u_r\mathbf{e}_r + u_\theta\mathbf{e}_\theta) = -wu_\theta\mathbf{e}_r + wu_r\mathbf{e}_\theta$$

$$q_H = \nabla.\mathbf{l} = -4\mathbf{\Omega}^2\mathrm{e}^{-r^2/a^2}(2e^{-r^2/a^2} - 1)$$

The hydrodynamic charge is negative inside the core and is balanced mostly by a positive charge near the edge of the core around $r \sim a$ (see below for the comparison with experiments). Strictly speaking, the hydromagnetic charge is negative for $(r/a)^2 < \ln 2$ and positive for $(r/a)^2 > \ln 2$. For comparison, the Rankine vortex has a rigid rotation core inside which $\nabla.\mathbf{l} = -4\Omega^2$ and at the edge of the core, there is an opposite delta function charge distribution. In any case, one expects the total charge per unit height ($\Delta z = 1$) to vanish over the plane:

$$\Delta q = \int_0^\infty q_H 2\pi r\mathrm{d}r = 0$$

Hence, the charge is truly a topological feature of the flow if we remind that topology is, by definition, the study of those properties of geometric forms that remain invariant under certain transformations. The total charge of a vortex is constant. We were able to display a new invariant quantity in the theory of fluid mechanics like, for example, the helicity for a perfect flow.

In the rest of the paper we study experimentally a Burgers vortex. From particles images velocimetry (PIV) measurements we extract the Lamb vector field and compute the hydrodynamic charge. Then, we implement a numerical Helmholtz–Hodge decomposition of the associated Lamb vector field.

3 Experimental measurements

The setup consists of a single stirring rod of 40 mm diameter, 110 mm in length, rotating at the bottom of a water cell. The cell is cylindrical with 290 mm inside diameter and 350 mm height, and closed from above by a transparent perspex plate in complete contact with the water. The tip of the rod is trimmed as a four-blade stirrer extending to the diameter of the rod where the blades are flat 3 mm thick and 20 mm high (see Fig. 1). The measured flow was produced with rod rotation speed of seven rounds per second.

The flow is measured by particle image velocimetry (PIV) at the plane 45 mm above the rotating tip using 2 mm thick light sheet from a double pulse laser (SoloPIV 532 nm from New-wave research). The separation time between pulses is fixed at 1 ms. A double frame camera of 1 Mpx is located above the cell. The analysis program is based on multipass correlation algorithm, written by Enrico Segre. The resulting instantaneous velocity field is determined on 80×80 vector grid. The velocity fields were acquired at a rate of 4 Hz during 38 s.

From the PIV measurements, one infers the velocity field and computes the radial profile of the azimuthal velocity field (Fig. 2a, b). The fitted parameters according to the Burgers model are $\Omega = 86$ rad/s, and $a = 9.2$ mm. For all plots, the scaling is linear and the pictures are averaged over all acquired images. Without averaging, the plots are very similar. We used averaging in order to smooth the data for computation purposes especially for the Helmholtz decomposition. The error bars in Fig. 2b, d, and f are based on a comparison with similar results of another set of measurements (performed at 480 rpm rotation speed, with velocities scaled according to the rotation speed difference by 540/480). The vertical vorticity shown in Fig. 2c and d is deduced from the velocity field. The hydrodynamic charge is displayed in Fig. 2e and f. One notices that the negative core is surrounded by a positive annulus of charge that decays farther outside to zero similarly to the Lamb vector. However, the total charge in the frame integrates to an average charge of about –200 l/s^2. The charge is completely balanced only at the wall of the cell, due to a circulation residue. Despite the fact that the structure of the vortex bears ressemblance with the Burgers vortex, the tail of the vortex cannot look like the one in an infinite open space.

The radial profiles of the vorticity and the charge compare reasonably with the calculations of the Burgers vortex with the same parameters as above. The apparent deviations between experiment and theory in Fig. 2f can be explained by viscous effects, which tend to smooth out the velocity profile hence all derived quantities like the Lamb vector and the charge especially at the outer edge of the vortex where the velocity reaches a maximum. Moreover, the center of the vortex is not fixed so, in each frame, the radial profile is determined with different reference points. Possibly, the advection of vorticity is not left without trace and part of the coherence of the structure is destroyed either by the sampling average or by a dynamical mechanism in the flow. This means that the local charge is smoothed in the center and does not display an ideal vortex structure.

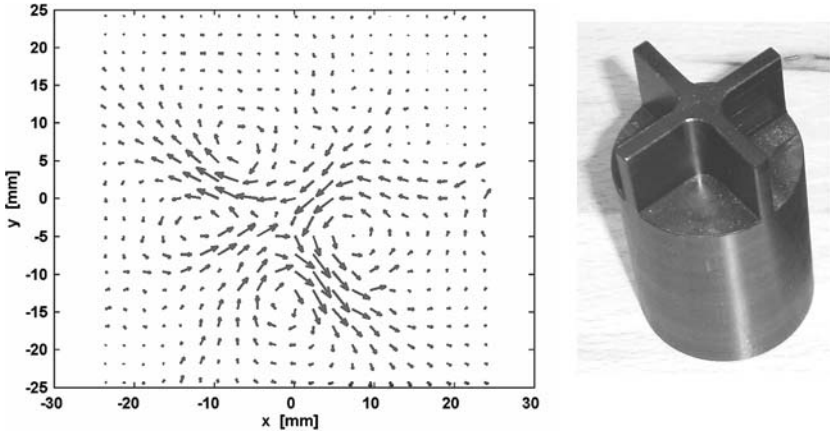

Fig. 1 (Experimental vortex) a snapshot of the divergence-free part of the Lamb vector and the rotating rod tip that may explain the peculiar symmetry

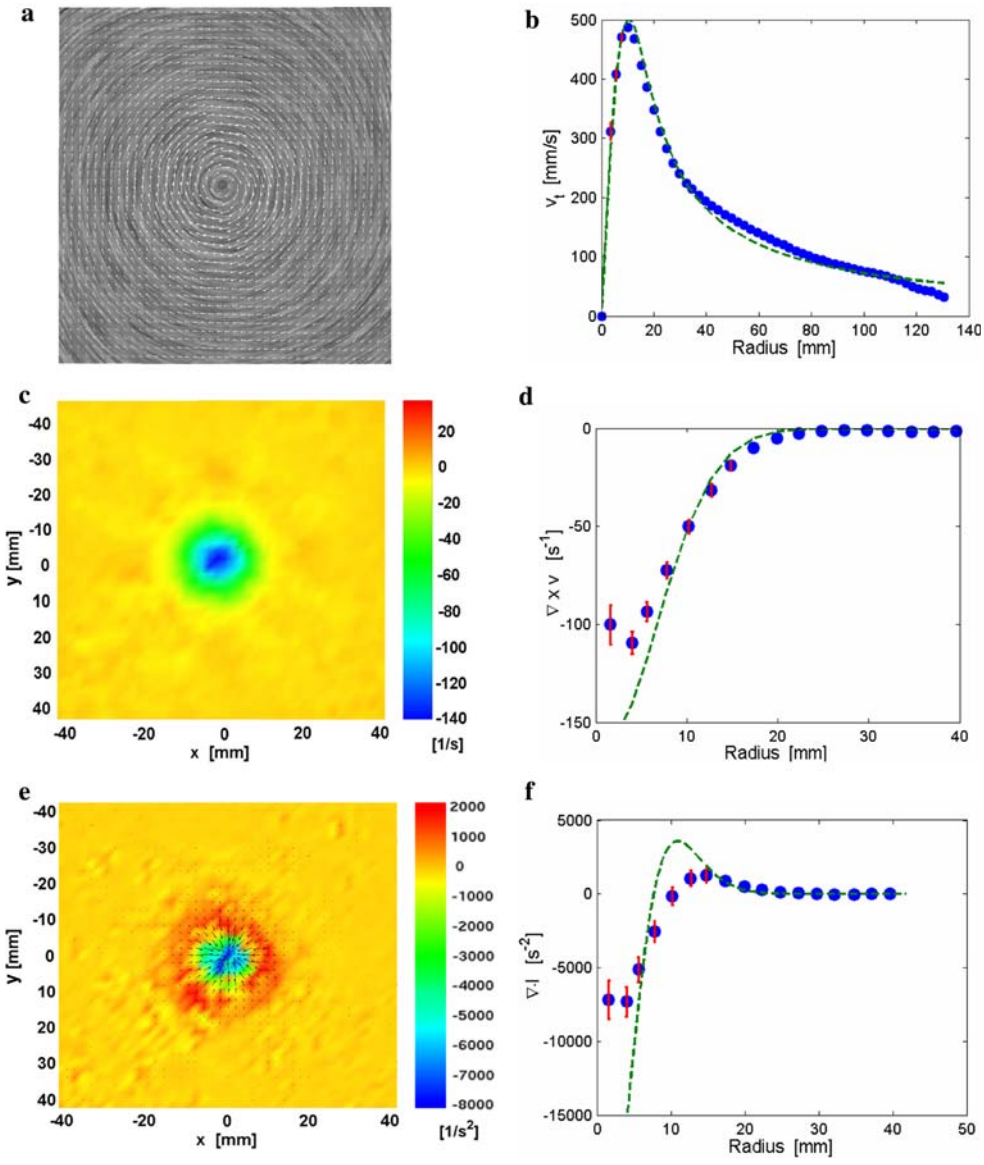

Fig. 2 (Colour online): (experimental vortex) **a** Velocity field and its LIC visualisation (LIC is the line integral convolution), **b** radial profile of the azimuthal velocity, **c** vertical vorticity (in s^{-1}), **d** radial profile of the vertical vorticity, **e** planar Lamb vector and planar hydrodynamic charge (in s^{-2}), **f** radial profile of the hydrodynamic charge. The profile fits are based on the Burger model. Error bars are displayed in *red*

4 Discrete Helmholtz–Hodge decomposition

As mentioned above, we use the Helmholtz–Hodge decomposition to separate the Lamb vector into an irrotational and a solenoidal part. The decomposition is implemented in a way similar to Tong et al. (2003).

The discrete Helmholtz–Hodge decomposition of the Lamb vector l tries to mimic the smooth decomposition described by $l = d + r + h = \nabla D + \nabla \times R + h$. Here d and r are the irrotational and the solenoidal part respectively. The so-called harmonic part h is both irrotational and solenoidal. As in 2D the curl is not a vector we have to rewrite the decomposition for 2D as $l = d + r + h = \nabla D + J\nabla R + h$ where $J\nabla$ is the co-gradient and J rotates every vector by 90° in counter clockwise order (see Polthier and Preuß 2002). One easily verifies that the divergence of $r = J\nabla R$ vanishes and thus r is solenoidal in the two dimensional case too. The harmonic part can be added to d or r without changing their main characteristic (solenoidal / irrotational). Thus the decomposition can be written as previously: $l = d' + r' = \nabla\alpha + \nabla \times \beta$.

In the smooth case ∇D and $\nabla \times R$ correspond to projections of l onto the spaces of curl-free resp. divergence-free vector fields. Such projections can be achieved by minimizing the following functionals:

$$F(D) = \frac{1}{2}\int_T (\nabla D - l)^2 dV$$

$$G(R) = \frac{1}{2}\int_T (J\nabla R - l)^2 dV$$

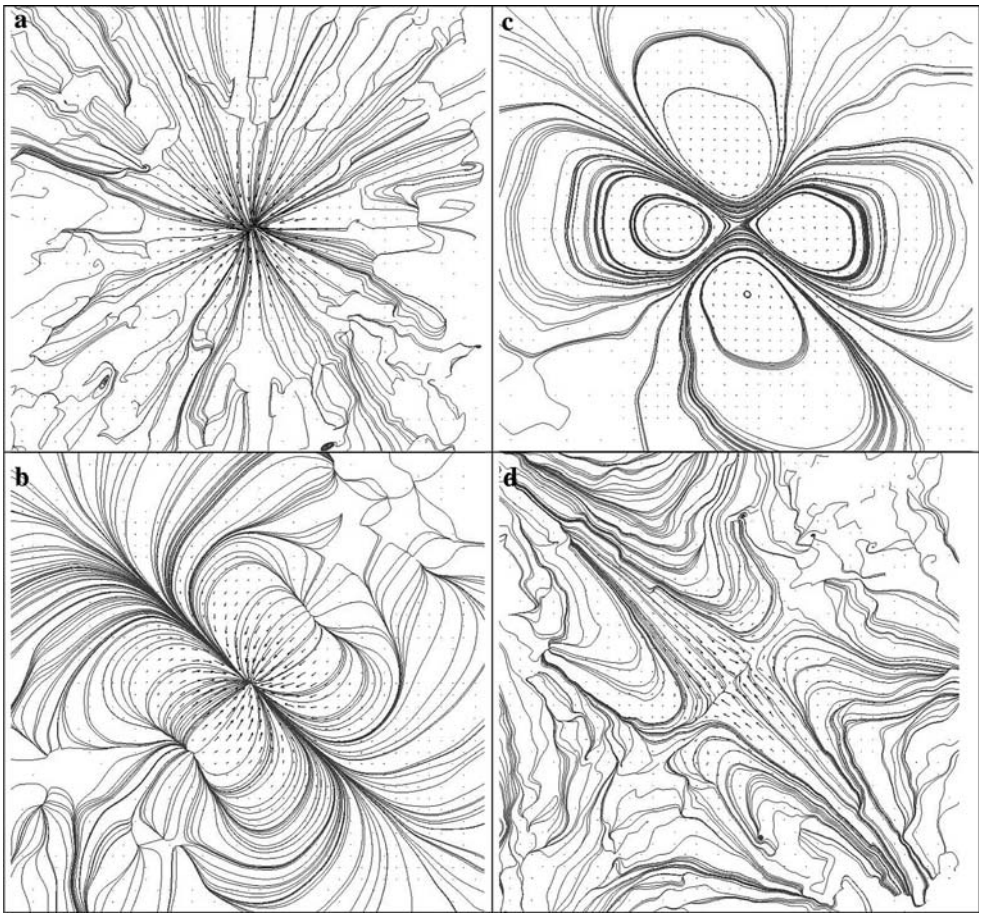

Fig. 3 (Experimental vortex) **a** Planar Lamb vector field and its streamlines, **b** divergence-free part of the Lamb vector, **c** vorticity free part of the Lamb vector, **d** harmonic part of the Lamb vector

Trying to mimic the smooth case, the two potentials D and R are derived by projections in the discrete case too; see Tong et al. (2003) for details. Discretization of the above equations leads to a sparse linear system for each potential. To guarantee unique solutions, boundary conditions have to be specified. We follow Tong and choose the boundaries of the potentials to be zero. With this choice d is orthogonal to the boundary and r is tangential to it.[1] To solve the sparse systems, we employ a standard conjugate gradient method. The solution vectors contain the values of the potentials for each point. Computing the gradient and the co-gradient respectively yields the desired components of the field l.

Since the decomposition is a global variational approach and as the potentials are computed by integrated values, the decomposition has smoothing effects on the results. This is valuable as we are working with measured data.

For all plots in Fig. 3, the streamlines associated to each type of vector are started at randomly distributed points. The Lamb streamlines are emitted from the centre of the vortex. If the Lamb vector was only a gradient the streamlines should be star-like. However, we notice for our experimental vortex a small spiralling behaviour. Hence, we infer the presence of, at least, a transverse part of the Lamb vector, which indeed looks like a four-leaved clover, which reminds us the symmetry of the stirrer (Fig. 1). In addition, both the divergence-free and the harmonic part of the Lamb vector are asymmetric.

The spiralling behaviour is due to the presence of the radial and vertical components of the velocity, which do create a transverse component of the Lamb vector. Quoting Saffman (1992, p. 47): " If in a steady flow, $\boldsymbol{l}$ is not the gradient of a single valued scalar, which can be absorbed in the pressure, then an external body force must be applied to maintain equilibrium". In the present experiment, this is the spinning axis and propeller. The motion is accompanied by a radial and an axial velocity. We checked experimentally using the Burgers model that the azimuthal component of the Lamb vector is very small compared to its radial part as the former one is proportional to the kinematic viscosity:

[1] To avoid confusion, note that all figures show only a cut-out of the whole field. The boundary is not shown.

$$\mathbf{l}_{//} = -\frac{2\boldsymbol{\Omega}^2 a^2}{r}\mathrm{e}^{-r^2/a^2}\left(1-\mathrm{e}^{-r^2/a^2}\right)\mathrm{e}_r >>$$
$$\mathbf{l}_{\perp} = -\frac{4\nu\boldsymbol{\Omega}}{a^2}\mathrm{e}^{-r^2/a^2} r\mathbf{e}_\theta$$

5 Criteria for detection of the vortex centre

In order to compare the criterion based on the Lamb vector and the hydrodynamic charge (see Fig. 2e, f) with one of the considered before criteria, namely Q-criterion, let us first relate these two criteria. Indeed, the hydrodynamic charge can be easily computed with the gradient of the kinetic energy and the Q-criterion via the following expressions:

$$\nabla.\mathbf{l} = -\nabla^2\left(\frac{p}{\rho}+\frac{\mathbf{u}^2}{2}\right) = -2Q - \nabla^2\left(\frac{\mathbf{u}^2}{2}\right) = q_H$$

hence:

$$Q = -\frac{1}{2}\left(q_H + \nabla^2\left(\frac{\mathbf{u}^2}{2}\right)\right)$$

The vortex cores are usually characterized by strong positive values of Q (as the pressure reaches a minimum in the centre) and we can identify the vortex cores as the circular regions with positive Q around a peak of vorticity. As discussed previously, the hydrodynamic charge takes into account both the influence of pressure (Q) and the influence of velocity. Indeed, the vortex centre corresponds to a local minimum of these two quantities. The Q-criterion captures only minima of pressure. Hence, the hydrodynamic charge is a kind of modified Q-criterion that takes into account also the influence of the kinetic energy.

In Fig. 4a, we superimposed visualizations of the Lamb vector and the hydrodynamic charge fields. This image actually reproduces the same data and in the same form which is shown in Fig. 2e but obtained by a different numerical procedure via a discrete Helmholtz–Hodge decomposition. Figure 4b presents the following data: the color and color-bar visualize the field of div(grad(**u**/2)), the scaled arrows show grad(**u**/2), the line integral convolution (LIC) in the background shows the structure of grad(**u**/2), the dots with the white lines show the topology of grad(**u**/2). The red squares are saddle points and the black squares are sinks. Both are zeros of the vector field displayed. In Fig. 4c, the Q-criterion is presented. One can learn from the images that the hydrodynamic charge and the Lamb vector fields characterize the vortex in the clearest way.

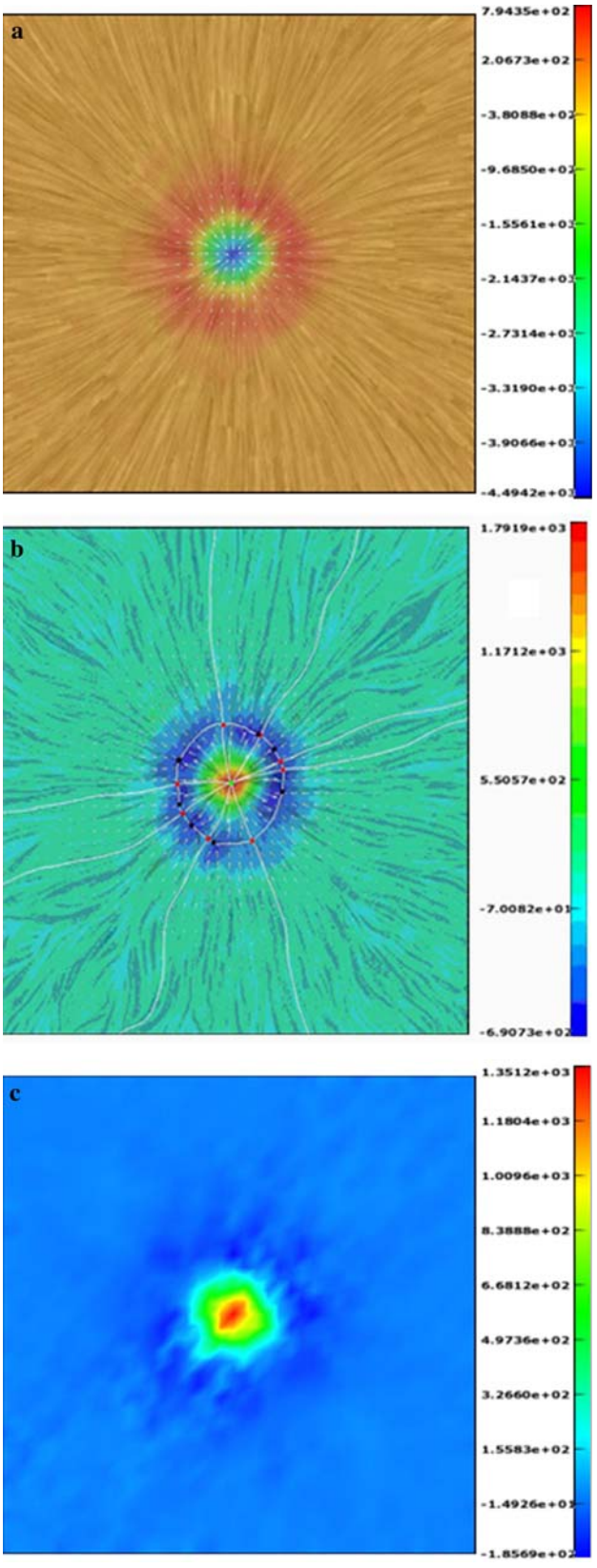

Fig. 4 (Color online): (experimental vortex) **a** Hydrodynamic charge, **b** gradient of the kinetic energy, **c** Q-criterion = Laplacian of the pressure

6 Vortex dynamics characterization

An immediate and useful application of the Lamb vector and hydrodynamic charge concepts is to study the dynamics of coherent structures in a turbulent flow. As an example, we examined first movies of PIV images by using the divergence-free (solenoidal) part and rotational-free part of the Lamb vector field and found a clear episode pattern. Ordinarily, in the rotational-free part we observe a cloud of vectors pointing towards the centre of the vortex (the direction does not change in either rotation direction of the vortex). Only occasionally we observe events when the vortex breaks into separate hydrodynamic charges. A cloud emerges with outward pointing vectors beside the inward pointing vectors cloud, but in the next frame the ordinary situation is recovered (see Fig. 5). In the solenoidal picture of such events, we observe disturbances with high magnitudes.

In order to identify numerically the occurrence of special events, we describe two results of analysis by intuitive names as the ''polarity'' and the ''EMF'' (electro-motive force). The polarity is the difference between the maximal positive charge and the maximal negative charge observed in the frame (the charge is the divergence of the rotational-free part of the Lamb vector). The EMF is the net value of the solenoidal part of the Lamb vector, presented as the magnitude of the averaged vector over the entire frame. As we have shown for a single eddy, the solenoidal part of the Lamb vector is related to the time derivative of the global vorticity (that is analogous to the time derivative of a magnetic flux that produces EMF). The vorticity is summed to zero in a large enough fluid volume. In this case, the total circulation around the cell must be zero, and the wall of the cell provides a part of the negative vorticity. We do not include the wall in the analysis frame in the same way that one does not include magnetic flux outside a coil in its EMF calculation. Accordingly in Fig. 6, we show the trajectory of the vortex centre in x-y coordinates (which determination is based on the Lamb vector and the hydrodynamic charge criterion), the polarity and the EMF (in arbitrary units) versus time. Clearly, there are specific events that are identified by peaks in both the polarity and EMF plots. For example, the episode shown in Fig. 5 relates to the first peak at $t = 0.75$ s. In addition, there is a correlation between the peaks and abrupt changes in the course of the vortex trajectory, as marked by arrows in the Fig. 6. One can also notice that large EMF peaks predict large instability of the trajectory (indicated by larger displacements). This analysis demonstrates the usefulness of the approach to identify the vortex core and to provide detail informations about the dynamics of coherent structures that has been unavailable before.

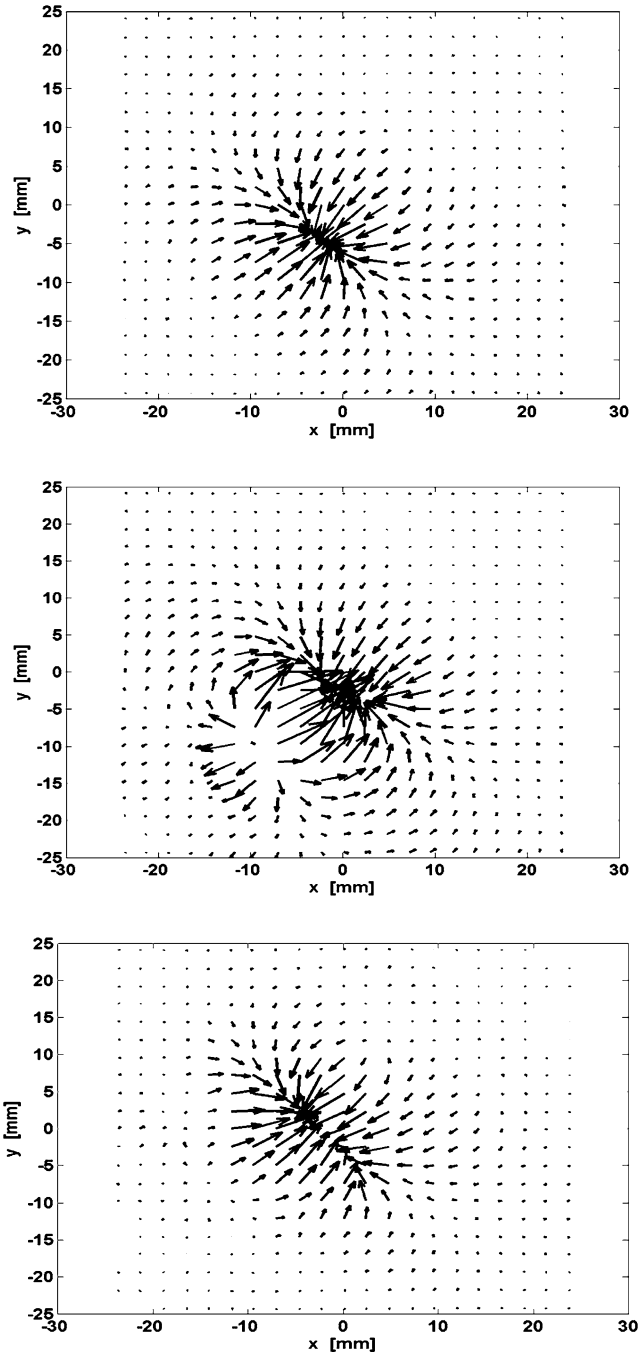

Fig. 5 (Experimental vortex) a typical episode of spontaneous disturbances in the vortex shape and course as observed in the irrotational part of the Lamb vector ($t = 0.5, 0.75, 1$ s)

7 Conclusions and perspectives

In this paper we demonstrate the usefulness and effectiveness of the concepts of the Lamb vector and the

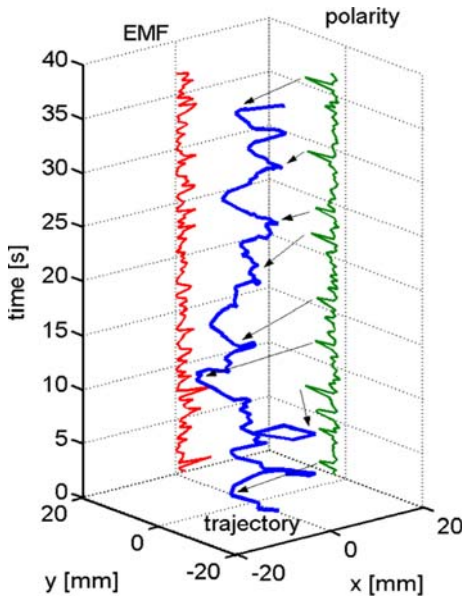

Fig. 6 (Color online): (experimental vortex) summary of correlated quantities in vortex dynamics for spontaneous disturbances: the centre position of the vortex, the polarity, and EMF versus time (see definitions in text). *Arrows* indicate the point of the event on the 3D plot of the trajectory

hydrodynamic charge to locate and characterize coherent structures such as a vortex on the experimental data. In addition, the topology of the Lamb vector seems also to be a rather robust indicator for the presence of coherent structures particularly by applying the Helmholtz–Hodge decomposition. We have shown that the total charge is conserved both for the Rankine and the Burger vortices, which are canonical examples of model for coherent structures. The hydrodynamic charge criterion was compared with the so-called Q criterion and includes in addition to pressure effects, velocity effects in the localization of coherent structures.

However, the scope of our results is limited as one needs to confirm such indications for more complicated situations such as described in the numerical simulations of Kollmann for a swirling jet in 3D (Kollmann and Umont 2004, Kollmann 2006). From the experimental point of view, 3D-PIV seems to be a good candidate in order to explore more deeply the role of the Lamb vector and its divergence in our understanding of coherent structures in turbulence.

Acknowledgments Two of us (Sh. S. and V. S.) are grateful to E. Segre for providing us a multi-pass correlation algorithm and for his help in software support. This work is partially supported by grants from Israel Science Foundation, Binational US–Israel Foundation, and by the Minerva Centre for Nonlinear Physics of Complex Systems. G.R. was financially supported by a grant ''post-doc CNRS'' (S.P.M. section 02) during his post-doctoral stay in Nice. A.W. was supported by DFG grant SCHE 663/3-7.

References

Clerk Maxwell J (1873) A treatise on electricity and magnetism. Clarendon Press

Douady S, Couder Y, Brachet ME (1991) Direct observation of the intermittency of intense vorticity filaments in turbulence. Phys Rev Lett 67:983–986

Dubief Y, Delcayre F (2000) On coherent vortex identification in turbulence. J Turbul 1:011

Haller G (2005) An objective definition of a vortex. J Fluid Mech 525:1–26

Kirby RM, Marmanis H, Laidlaw DH (1999) Visualizing multivalued data from 2d incompressible flows using concepts from painting''. Proceedings of IEEE visualization 1999, San Francisco, CA

Kollmann W (2006) Critical points and manifolds of the Lamb vector field in swirling jet. Comput Fluids 35(7):746–754

Kollmann W, Umont G (2004) Lamb vector properties of swirling jets. Fifteenth Australasian fluid mechanics conference, Sydney, Australia, pp 13–17 available from http://www.aeromech.usyd.edu.au/15afmc/proceedings/papers/AFMC00081.pdf

Lamb H (1878) On the conditions for steady motion of a fluid. Proc Lond Math Soc 9:91

Lesieur M, Begou P, Briand E, Danet A, Delcayre F, Aider JL (2003) Coherent-vortex dynamics in large-eddy simulations of turbulence. J Turbul 4:016

Marmanis H (1998) Analogy between the Navier–Stokes equations and Maxwell's equations: application to turbulence. Phys Fluids 10:1428–1437

Polthier K, Preuß E (2002) Identifying vector field singularities using a discrete hodge decomposition. In: Hege H-C, Polthier K (eds) Visualization and mathematics III. Spinger, Berlin Heidelberg New York

Pumir A (1994) A numerical study of pressure fluctuations in three-dimensional, incompressible, homogeneous, isotropic turbulence. Phys Fluids 6:2071–2083

Saffman PG (1992) Vortex dynamics, Cambridge University Press

Shridar S (1998) Turbulent transport of a tracer: an electromagnetic formulation. Phys Rev E 58:522–525

Shtilman L (1992) On the solenoidality of the Lamb vector. Phys Fluids A 4:197–199

Speziale CG (1989) On helicity fluctuations and the energy cascade in turbulence. In: Koh SL, Speziale CG (eds) Recent advances in engineering science. Lecture notes in Engineering, pp 39–10

Sposito G (1997) On steady flows with Lamb surfaces. Int J Eng Sci 35:197–209

Tong Y, Lombeyda S, Hirani AN, Desbrun M (2003) Discrete multiscale vector field decomposition. SIGGRAPH 2003 Proceedings, ACM

Weiss J (1991) The dynamics of enstrophy transfer in two-dimensional hydrodynamics. Physica D 48:273

Wu J-Z, Ma HY, Zhou MD (2005) Vorticity and vortex dynamics. Springer, Berlin Heidelberg New York

Wu J-Z, Zhou Y, Fan M (1999a) A note on kinetic energy, dissipation, and enstrophy. Phys Fluids 11:503–505

Wu J-Z, Zhou Y, Lu X-Y, Fan M (1999b) Turbulent force as a diffusive field with vortical sources. Phys Fluids 11:627–635